Key Engineering Materials
ISSN: 1662-9795, Vol. 926, pp 1007-1020
doi:10.4028/p-u7u5i8

Submitted: 2021-12-08
Revised: 2022-01-21
Accepted: 2022-02-04
Online: 2022-07-22

Influence of the Anisotropic Behavior on Equibiaxial Paths

F.F. Salles[1,a*], M.C. Oliveira[1,b], D.M. Neto[1,c], J.L. Alves[2,d], L.F. Menezes[1,e] and J.V. Fernandes[1,f]

[1]CEMMPRE, Department of Mechanical Engineering, University of Coimbra, Portugal

[2]CMEMS, Department of Mechanical Engineering, University of Minho, Guimarães, Portugal

[a]uc2018269307@student.uc.pt, [b,c,e,f]marta.oliveira, diogo.neto, luis.menezes, valdemar.fernandes@dem.uc.pt, [c]jlalves@dem.uminho.pt

Keywords: Numerical simulation, Anisotropic metallic sheets, Stress and strain paths

Abstract. Marciniak and Nakajima tests are commonly used in building FLD's, since they allow covering all regions from uniaxial to almost equibiaxial strain paths. In this work, the deviation from equibiaxial strain paths is analyzed as function of the material anisotropic behavior. The numerical results show that material with $r_0 = r_{90}$ present equibiaxial stress and strain paths, while for the ones with $r_0 \neq r_{90}$ the paths are neither equibiaxial in stress nor strain. Moreover, it is shown that despite the similarities between the two tests, they present different sensitivity to the control of the blank holder force and to the friction coefficient. Namely, the stress and strain paths in the Marciniak specimen center are more sensitive to the control of the blank holder force. On the other hand, the stress and strain paths in the Nakajima specimen center are more sensitive to the friction coefficient. The deviation from the equibiaxial strain path indicates that the stress ratio is also not necessarily 1.0, meaning that the stress triaxiality and the Lode parameter also present some deviation from the reference values for an equibiaxial stress state. This should be taken into account when analyzing forming limit results.

Introduction

Sheet metal forming process are widely used by the automotive industry. Therefore, the numerical simulation of these processes has been continuously developed, since it allows predicting several forming defects, saving time and costs with prototypes and experimental tests [1,2]. Accordingly, several numerical models have been developed using the finite element method for modelling the elastoplastic behavior of the sheet metal under contact with the forming tools [3]. The accuracy of these models is strongly connected with the experimental data used in their calibration.

Among the most common failures in sheet metal forming processes, the strain localization that occurs before the ductile fracture of the material is one of the most important to be able to predict [4]. This phenomenon is commonly experimentally assessed using the Forming Limit Diagram (FLD), which was first proposed by Keeler and Goodwin [5,6]. Both the Marciniak and the Nakajima tests are used to define the forming limit curve, described by the ISO 12004-2 standard [7]. The circular specimen used in those experimental tests is intended to provide the equibiaxial stress state, such as in the hydraulic bulge test. However, it has been shown that for materials with a high degree of anisotropy, the material experiences a strain path that is neither equibiaxial in stress or strain, in the hydraulic bulge test [8,9]. This work aims to analyze the behavior of virtual materials with different degrees of anisotropy in Marciniak and Nakajima tests.

Marciniak tests. This test was proposed by Marciniak [10] and it is performed using a flat punch, as shown in the Fig. 1. The blank is lubricated but in order to minimize the influence of the lubrication conditions, an intermediate blank, with a circular hole, is placed between the punch and the metallic specimen. This guarantees that fracture occurs in the material located in the planar bottom of the cup. In order to obtain different strain paths, punches with different cross sections can be used, such as circular, elliptical or rectangular. Nevertheless, the most used solution is to change the width of the specimen [11].

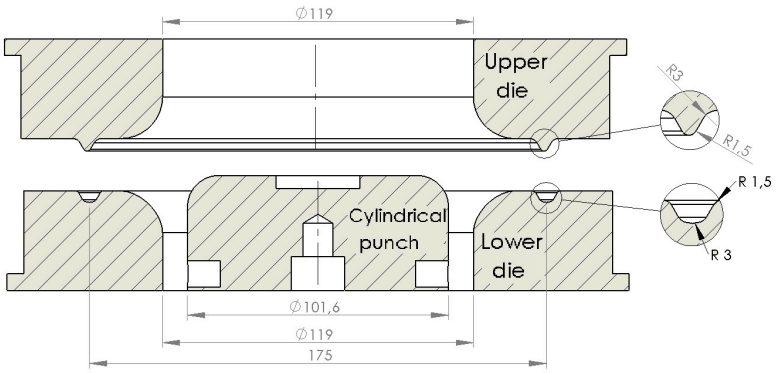

Figure 1. Schematic layout of the device used in the Marciniak test.

Nakajima tests. The Nakajima test uses a spherical punch and a circular die, as shown in Fig. 2 [11]. In order to generate different strain paths, the specimen geometry is modified, varying the width of the central region. As in the Marciniak test, the blank is lubricated to reduce the influence of the lubrication conditions of the test results. Nevertheless, it is known that the contact conditions between the punch and the blank alter the location of the strain localization [12].

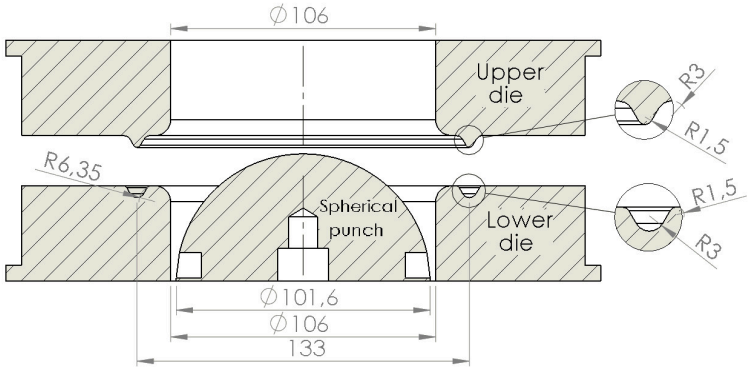

Figure 2. Schematic layout of the device used in the Nakajima test.

Numerical Model

Constitutive model. For metallic sheets, the elastic behavior is assumed as isotropic. The Hooke's law is adopted, which requires the definition of the Young's modulus, that for the virtual material used is E=210 GPa, and of the Poisson coefficient, υ=0.3. The plastic behavior is defined by a flow rule, a hardening law and a yield criterion [13]. In the current study, an associated flow rule is adopted, meaning that the yield criterion has the dual role of plastic potential. The hardening was described by the Swift law:

$$Y = K\left(\varepsilon_0 + \bar{\varepsilon}_{\mathrm{p}}\right)^n. \quad (1)$$

where Y is the flow stress and $\bar{\varepsilon}_{\mathrm{p}}$ is the equivalent plastic strain. ε_0, K and n are material parameters, with the latter being commonly referred as the strain-hardening coefficient [14,15]. The initial yield stress is defined as $Y_0 = K(\varepsilon_0)^n$. The parameters adopted in the numerical simulations are listed in Table 1.

The orthotropic behavior was described by the Hill 1948 yield criterion, which is a generalization of the Huber-Mises-Hencky isotropic criterion for anisotropic materials. The yield function is defined as follows [16]:

$$F\left(\sigma_y - \sigma_z\right)^2 + G(\sigma_z - \sigma_{\mathrm{x}})^2 + H\left(\sigma_{\mathrm{x}} - \sigma_{\mathrm{y}}\right)^2 + 2L\tau_{\mathrm{yz}}^2 + 2M\tau_{\mathrm{zx}}^2 + 2N\tau_{\mathrm{xy}}^2 = Y^2. \quad (2)$$

where F, G, H, L, M and N are the anisotropy coefficients. The subscripts x, y, and z are related with the material axis, i.e. to the rolling, transverse, and thickness directions of the metal sheet, respectively [15,16]. The virtual materials selected present different values for the *r*-values evaluated from uniaxial tensile tests performed with the specimen aligned with the rolling, diagonal and transverse directions, i.e. r_0, r_{45} and r_{90}. The labelling adopted for the materials is constructed using the *r*-values, i.e. $r_{0\_}\, r_{45\_} r_{90}$. The anisotropy parameters of the Hill 1948 yield criterion were determined based on

these values and assuming the condition that $G + H = 1$, i.e. the Swift law corresponds to the stress vs. plastic strain curve under uniaxial tensile test along the Ox axis. Table 2 shows the anisotropy coefficients of the virtual materials used in the simulations.

Table 1. Swift hardening law parameters.

Y_0[MPa]	K[MPa]	ε_0	n
200	577.08	0.005	0.20

Table 2. Hill48 criterion parameters of the virtual materials.

Material	*F*	*G*	*H*	*L*=*M*	*N*
1_1_1	0.500	0.500	0.500	1.500	1.500
0.6_3_0.6	0.625	0.625	0.375	1.500	4.375
1.5_3_1.5	0.400	0.400	0.600	1.500	2.800
1.5_3_3	0.200	0.400	0.600	1.500	2.100
0.6_1.8_3	0.125	0.625	0.375	1.500	1.725

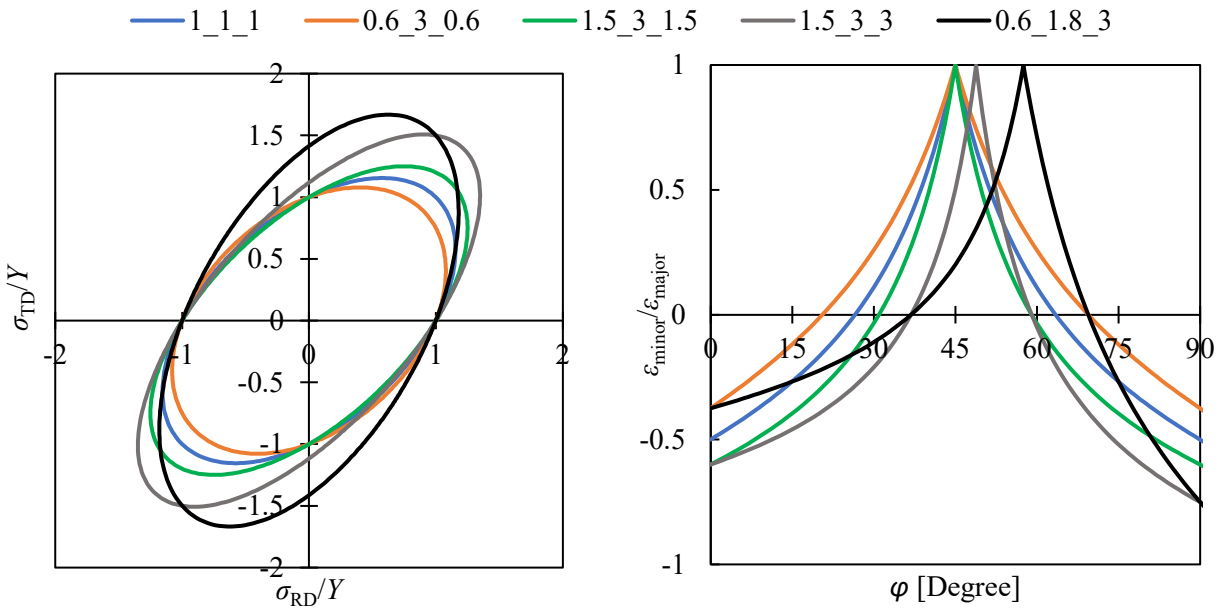

Figure 3. Mechanical behavior of the virtual materials: (a) normalized yield surface assuming plane stress conditions with the $\sigma_3 = 0$; (b) strain ratio evolution as a function of the loading direction.

Fig. 3 (a) presents the normalized yield surface for each material, highlighting that for the materials with r_0=r_{90} the major axis of the ellipse has a slope equal to 1.0, while the others have a higher slope. When analyzing plane stress states, it is common to define the loading direction, φ, based on the slope between the stress component in the transverse, σ_{TD}, and rolling directions, σ_{RD}. When adopting an associated flow rule, the normal to the yield surface defines the direction of the plastic strain rate. This enables the analytical evaluation of the ratio between the minor and major in-plane strains, $\varepsilon_{minor}/\varepsilon_{major}$. Fig. 3 (b) shows the evolution of this strain ratio as function of the loading direction (φ). Considering the equibiaxial stress condition (φ =45°), by definition all materials have a stress ratio (σ_{TR}/σ_{RD}) equal to 1. However, Fig. 3 (b) shows that only the materials with r_0=r_{90} will present $\varepsilon_{minor}/\varepsilon_{major}$=1 for φ =45°. The materials with $r_0 \neq r_{90}$ present a value for $\varepsilon_{minor}/\varepsilon_{major}$ smaller than 1, which is attained only for higher values of φ, in agreement with the increase of the slope of the major axis of the ellipse. Thus, for materials with r_0=r_{90} the equibiaxial stress and strain path occur for φ =45°, while for the 1.5_3_3 the equibiaxial strain path correspond to φ =48.8° (σ_{TD}/σ_{RD}=1.14) and for 0.6_1.8_3, φ =57.5° (σ_{TD}/σ_{RD}=1.57). On the other hand, the equibiaxial stress state corresponds to a $\varepsilon_{minor}/\varepsilon_{major}$ ratio of 0.5 for the materials 1.5_3_3 and 0.2 for the 0.6_1.8_3.

Any stress state can also be characterized by the triaxiality and the Lode parameter. The stress triaxiality is the relative degree of hydrostatic stress, while the Lode parameter characterizes the magnitude of the intermediate principal stress, σ_2, with respect to the other two (σ_1 and σ_3). The equibiaxial stress state presents $\sigma_1 = \sigma_2 > \sigma_3 (= 0)$. Thus, the corresponding value for the stress triaxiality is 0.67 (2/3) while for the Lode parameter is -1. Note that when $\sigma_2 = (\sigma_1)/2 > \sigma_3 (= 0)$ the value of the stress triaxiality becomes lower (0.57 ($\sqrt{3}/3$)) and the Lode parameter is null. Thus, the increase of the ratio between the major and the minor in plane stresses leads to a reduction of both the stress triaxiality and the Lode parameter.

Finite element model. The evolution of the stress and strain paths in the Marciniak and Nakajima tests is studied using numerical simulations, performed with the in-house finite element solver DD3IMP (Deep Drawing 3D IMPlicit) [17,18]. In order to reduce the computational time, only a quarter of each test was modelled, taking advantage of the geometrical, loading and material symmetry conditions. The models included the draw bead geometry with the details given in Fig. 1 for the Marciniak test and in Fig. 2 for the Nakajima test. In this context, it should be mentioned that the intermediate blank was not considered in the Marciniak test, since this involves contact between deformable bodies. Instead, the geometry of the punch and lower die was offset with a value equal to the thickness of the intermediate blank, assuming that it suffers no deformation.

Considering one quarter, the blank's geometry is a square with dimensions: 101.6×101.6×1 (mm). The blank was discretized with linear hexahedral finite elements, combined with a selective reduced integration technique [19]. Two layers of elements were considered through the thickness to allow an accurate evaluation of the through-thickness stress gradients. The mesh of the blank presents structured zones with the element size defined based on the contact conditions with the tools. Unstructured finite element meshes were used for the transition regions, in order to make a smooth transition without element distortions. Moreover, a smaller element size was also applied in the central area of the blank, where the evolution of the stress and strain paths were followed. The Marciniak specimen has a total of 13500 elements while the Nakajima specimen has 12548. The blank rolling direction was always assumed to be oriented along Oy.

The forming tools are considered rigid and were modelled by Nagata patches [20,21]. The contact with friction conditions were modelled with the Coulomb friction model. Nevertheless, since the tests are commonly performed using lubricants to reduce friction, most of the numerical simulations were performed under frictionless conditions [22]. Most of the numerical simulations were performed with a closing force for the draw bead of 1280kN for the Marciniak test and 960 kN for the Nakajima test.

Results and Discussion

Influence of the orthotropic behavior. The Marciniak tests were performed for the different materials until attaining the maximum force, as shown in Fig. 4 (a). For the materials with $r_0 = r_{90}$, the punch force presents lower values for the 0.6_3_0.6 material, which has the smallest yield surface (see Fig. 3 (a)), while the opposite is observed for the 1.5_3_1.5. For the materials with $r_0 \neq r_{90}$, it is more difficult to correlate the results.

Fig. 4 (b) presents the strain paths observed at the specimen center for the different materials. Although materials 0.6_3_0.6 and 1.5_3_1.5 are anisotropic, the strain path is equibiaxial since $r_0 = r_{90}$. For the materials with $r_0 \neq r_{90}$, the strain path is no longer equibiaxial.

Fig. 5 (a) and (b) show the evolution of the stress triaxiality and the Lode parameter with the punch displacement, respectively. The triaxiality in all materials is close to the expected value for the equibiaxial stress state, i.e. 0.67 (2/3), except for the material 0.6_1.8_3, which has the highest degree of anisotropy. Similar results are seen for the Lode parameter, i.e. the materials present a value close to the expected one of -1. Nevertheless, the materials with $r_0 \neq r_{90}$ show some deviation, particularly the material 0.6_1.8_3, which is associated with a bigger difference between r_0 and r_{90}. As shown in Fig. 4 (b), the materials with $r_0 \neq r_{90}$ have a similar strain path, i.e. $\varepsilon_{\text{minor}}/\varepsilon_{\text{major}}$ ratio. Nevertheless, it corresponds to a loading direction (stress ratio) different from 45º, particularly for the material

0.6_1.8_3, as shown in Fig. 3 (b). The increase of the stress ratio justifies the differences in the values of the stress triaxiality and of the Lode parameter, observed in Fig. 5.

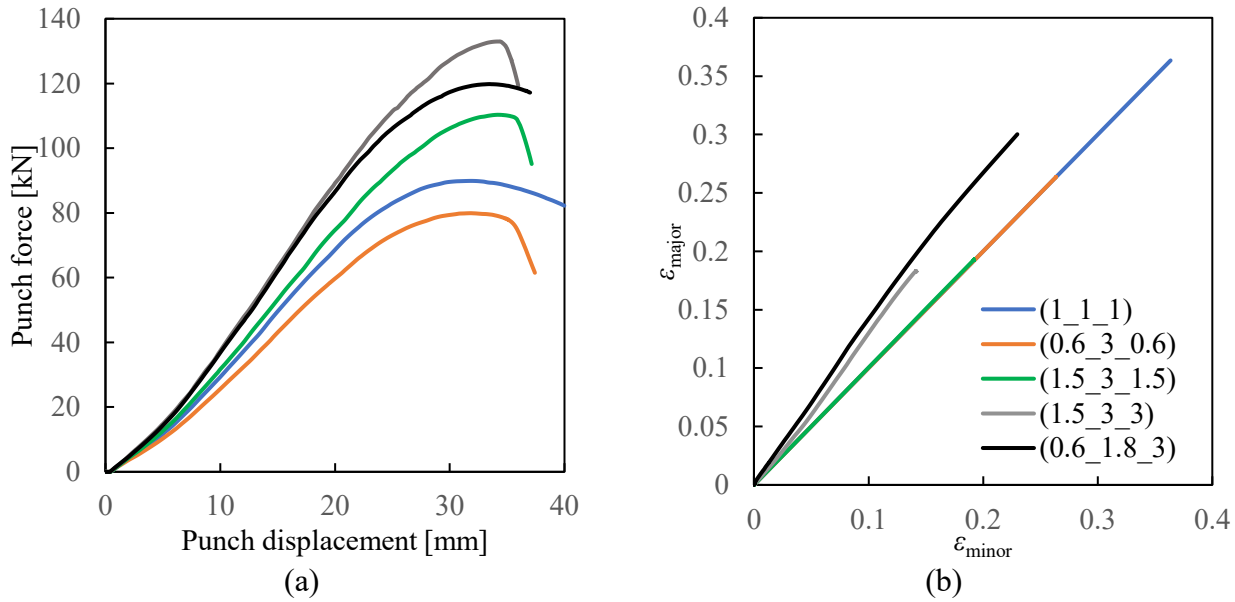

Figure 4. Effect of the material anisotropy on the predictions of the Marciniak test simulations: (a) punch force evolution; (b) major-minor strain.

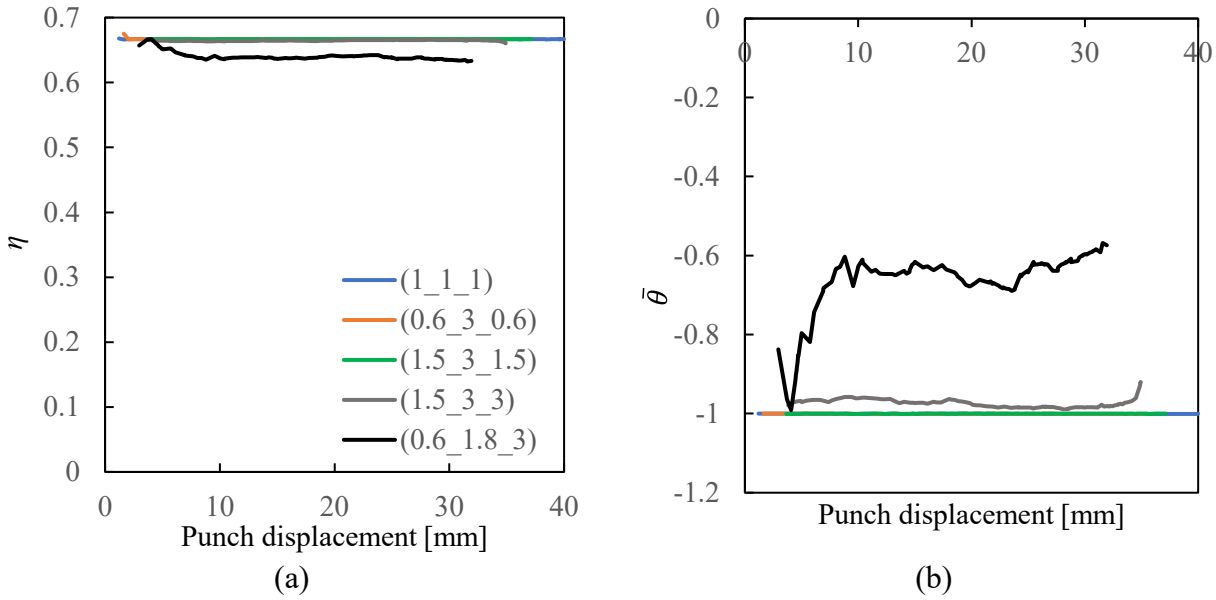

Figure 5. Effect of the material anisotropy on the predictions of the Marciniak test simulations: (a) Stress triaxiality; (b) Lode parameter.

Fig. 6 (a) and (b) show the evolution of the stress and strain ratios with the equivalent plastic strain, respectively. Only the materials 1.5_3_3 and 0.6_1.8_3 present ratios different from 1, i.e. the stress state found is neither equibiaxial stress nor equibiaxial strain. Taking into account the previous analysis of Fig. 3 (b), it is observed that for the material located in the center of the specimen the stress and strain paths are between these two. The loading directions are φ ~47.7° and φ =54.5° for the materials 1.5_3_3 and 0.6_1.8_3, respectively. It should be mentioned that the results are plotted only for the stage corresponding the punch displacement. Thus, the results highlight the fact that closure of the blank holder induces a higher pre-strain for the 1.5_3_3 material, when compared with the other materials.

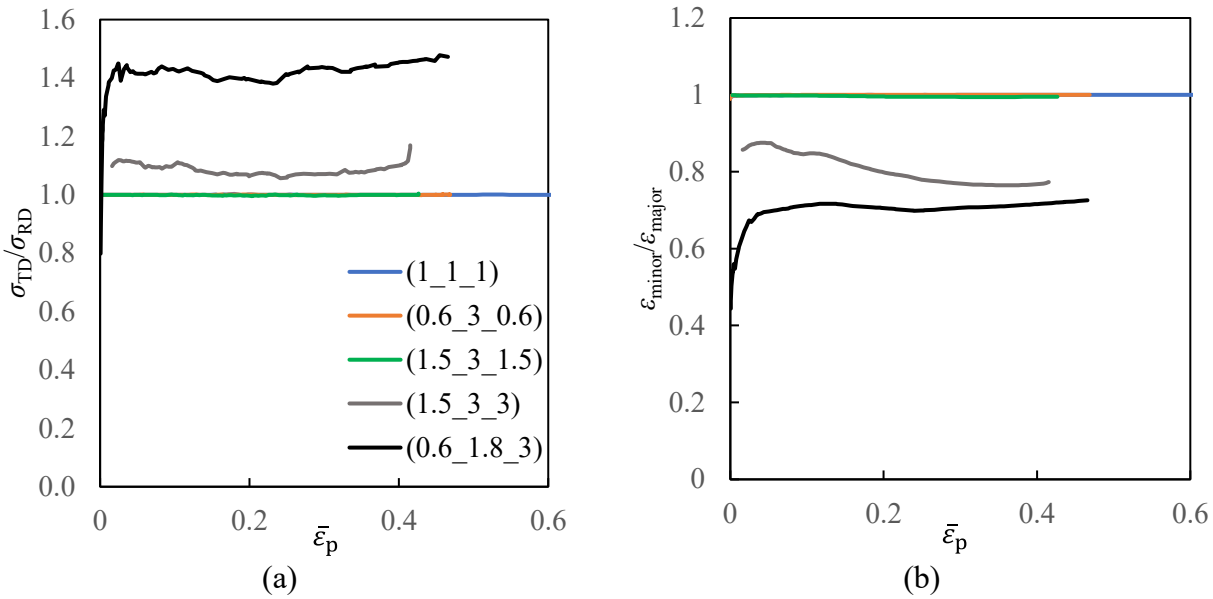

Figure 6. Effect of the material anisotropy on the predictions of the Marciniak test simulations: (a) Stress path ratio- equivalent plastic strain; (b) Strain path ratio- equivalent plastic strain.

Nakajima test were also performed for the different materials until a maximum punch displacement of 40 mm, as shown in Fig. 7 (a). The trend for the influence of the anisotropy in the punch force values is identical to the one observed for the Marciniak test (see Fig. 4 (a)). The lower punch force values are due to the spherical geometry of the punch used in the Nakajima test. The strain paths for all virtual materials are shown in Fig. 7 (b), showing that also in this case the equibiaxial strain state is only attained for the materials with $r_0 = r_{90}$. Since in this case higher values of equivalent plastic strain are attained, the slight deviation from a linear strain path is more evident for the materials with $r_0 \neq r_{90}$.

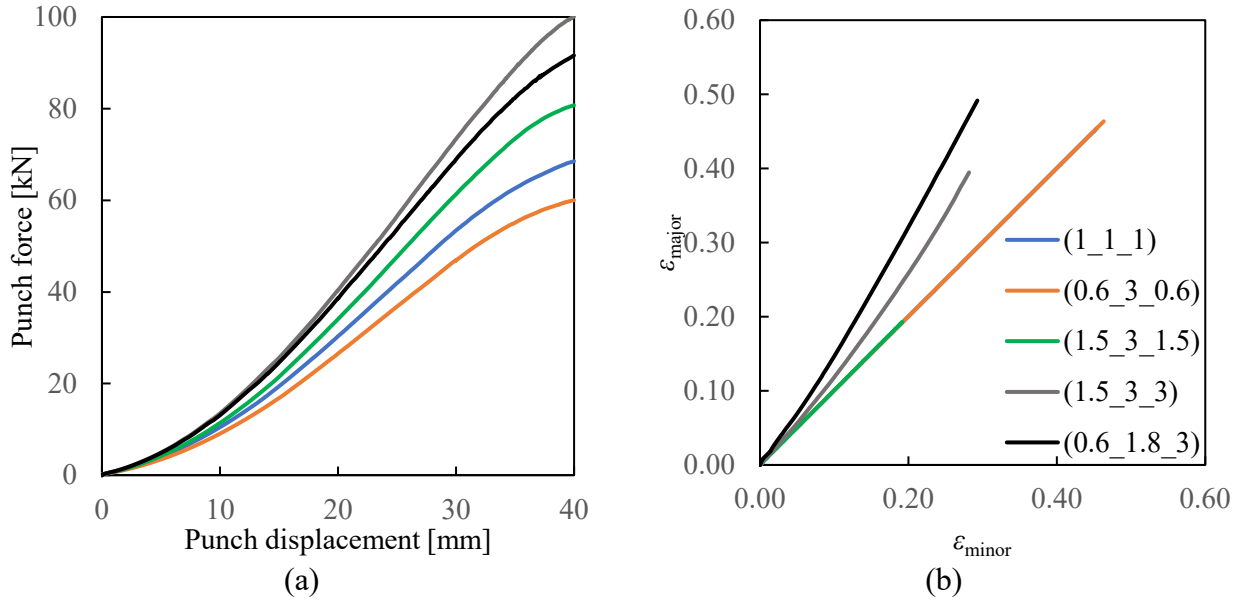

Figure 7. Effect of the material anisotropy on the predictions of the Nakajima test simulations: (a) punch force evolution; (b) major-minor strain.

Fig. 8 (a) and (b) show the evolution of the stress triaxiality and Lode parameter for all virtual materials studied. Also, in the case of these variables, the trend is very similar to the one observed for the Marciniak test, with a clear divergence from the reference values for the material 0.6_1.8_3. Note that the stress triaxiality and the Lode parameter are only plotted when the material enters in the plastic regime. Thus, the comparison of Fig. 8 with Fig. 5 highlights that the orthotropic behavior

also influences the punch displacement for which the materials enter in the plastic regime. The materials with the lowest values for the equibiaxial stress enter in plastic regime for lower values of punch displacement (see the normalized yield surfaces in the Fig. 3 (a)).

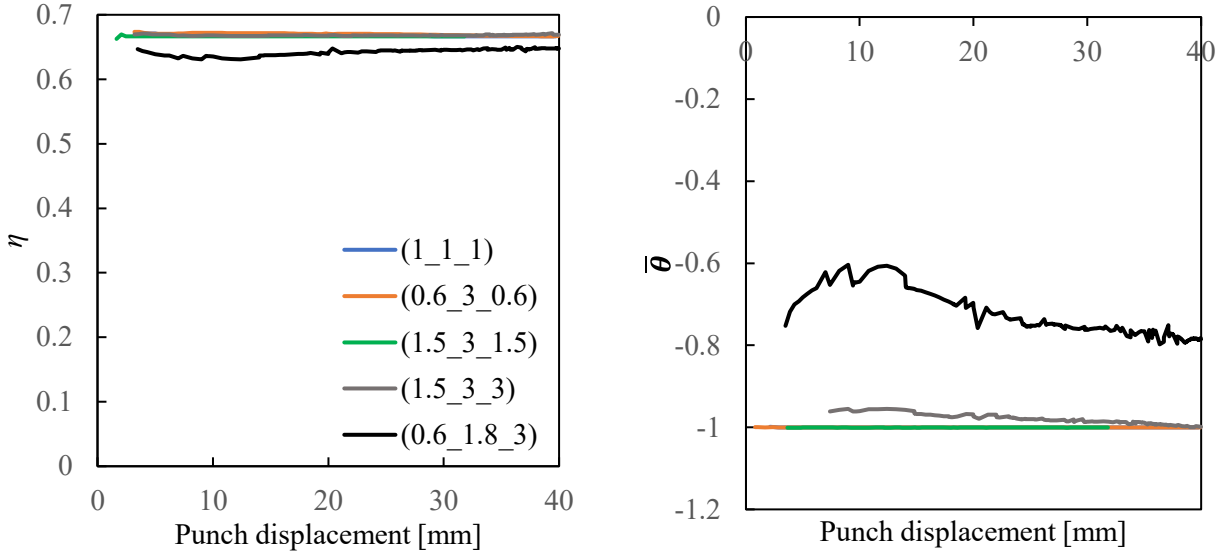

Figure 8. Effect of the material anisotropy on the predictions of the Nakajima test simulations: (a) Stress triaxiality; (b) Lode parameter.

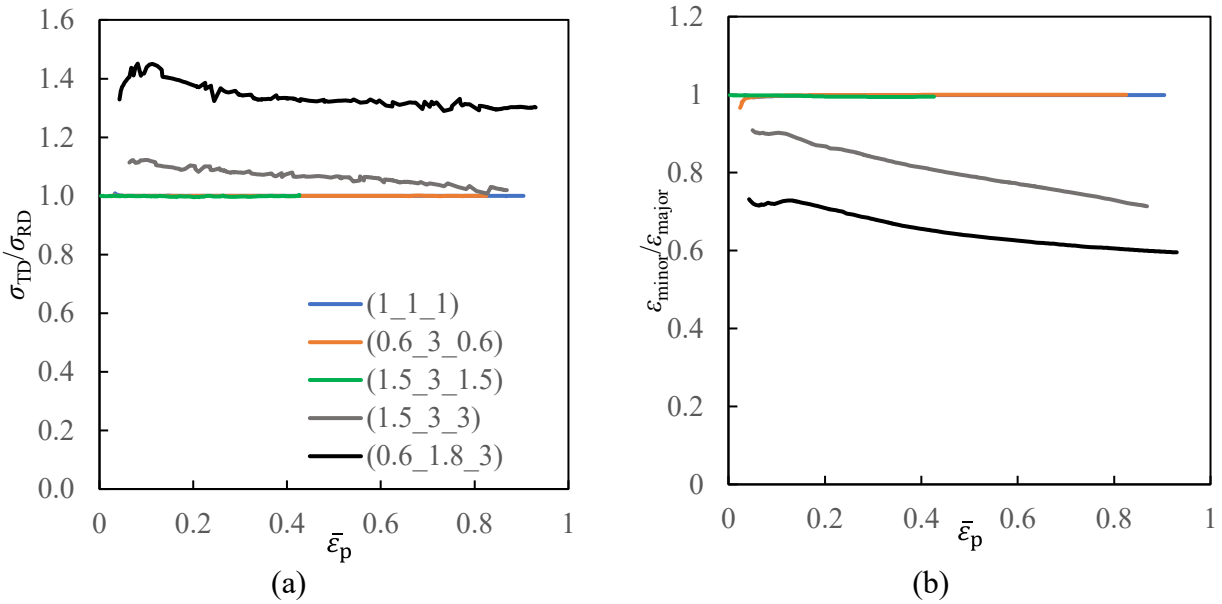

Figure 9. Effect of the material anisotropy on the predictions of the Nakajima test simulations: (a) Stress path ratio- equivalent plastic strain; (b) Strain path ratio- equivalent plastic strain.

Fig. 9 (a) and (b) show the evolution of stress ratio and strain ratio with the equivalent plastic strain for the Nakajima test. Although the results show a trend similar to the one observed in the Marciniak tests (Fig. 6), there are some relevant differences. In the Nakajima test, the closure of the blank holder induces a higher pre-strain for the materials 1.5_3_3 and 0.6_1.8_3. Moreover, both ratios present a linearly decreasing trend with the increase of the equivalent plastic strain, which is consistent with the slight change in the strain path observed in Fig. 7 (b). These results also show that it is more difficult to observe these slight changes in the evolution of the stress triaxiality than in the Lode parameter. Finally, for both tests the materials with $r_0 \neq r_{90}$ presented $\sigma_{\mathrm{RD}} \neq \sigma_{\mathrm{TD}}$ and $\varepsilon_{\mathrm{minor}} \neq \varepsilon_{\mathrm{major}}$, despite the geometrical constrains imposed by the circular draw bead. As expected the results are similar to those reported in [9] for the hydraulic expansion test.

Influence of the blank holder force. The analysis of the influence of the blank holder force is performed only for the material 0.6_1.8_3, since it presents the largest deviation from the equibiaxial stress state. Numerical simulations were performed only with blank holder forces lower than the one applied in the previous section.

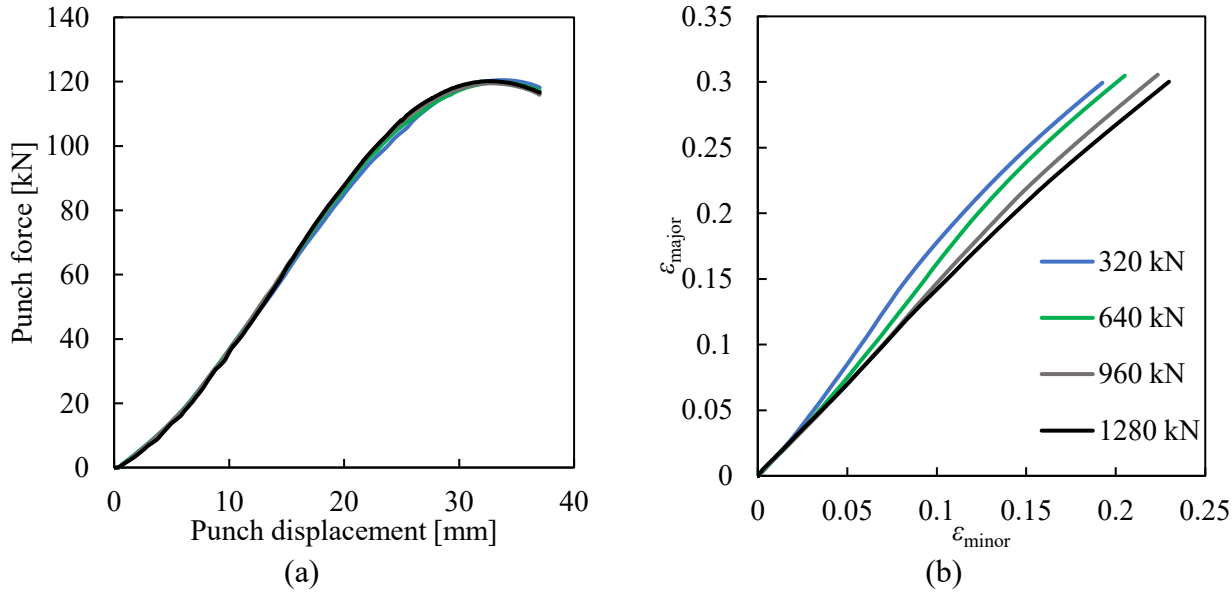

Figure 10. Effect of the blank holder force on the predictions of the Marciniak test simulations: (a) punch force evolution; (b) major-minor strain.

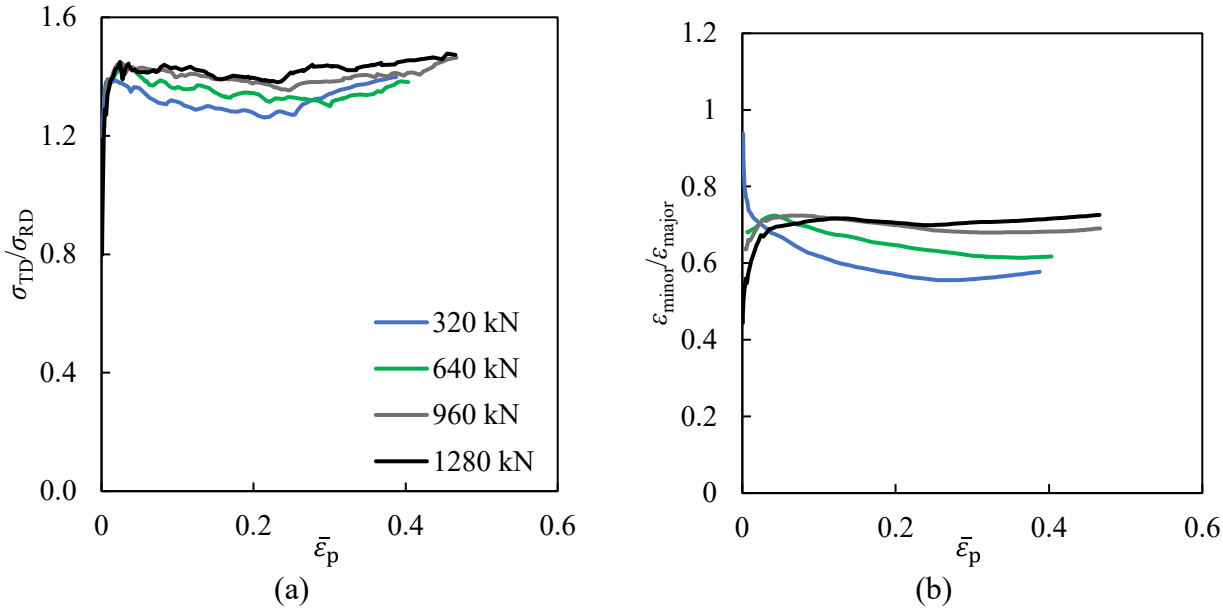

Figure 11. Effect of the blank holder force on the predictions of the Marciniak test simulations: (a) stress path ratio- equivalent plastic strain; (b) strain path ratio- equivalent plastic strain.

Fig. 10 (a) shows the Marciniak punch force evolution with its displacement confirming a negligible effect of the blank holder force. However, Fig. 10 (b) shows that there was a significant impact on the strain path, which is more linear when higher values are applied. In order to understand better these results, Fig. 11 (a) and (b) show the evolution of stress ratio and strain ratio. The impact caused by the increase of the force is visible, since it leads to an increase of the stress ratio to a value closer to 1.4 and the strain ratio to 0.7. Moreover, the paths become more constant. These results confirm the influence of the geometrical constrains imposed on the stress and strain states. Note that for a low blank holder force the stress ratio decreases and the material in the cup's center tends to deviate even more from the equibiaxial strain state, in agreement with the analysis presented in Fig. 3 (b).

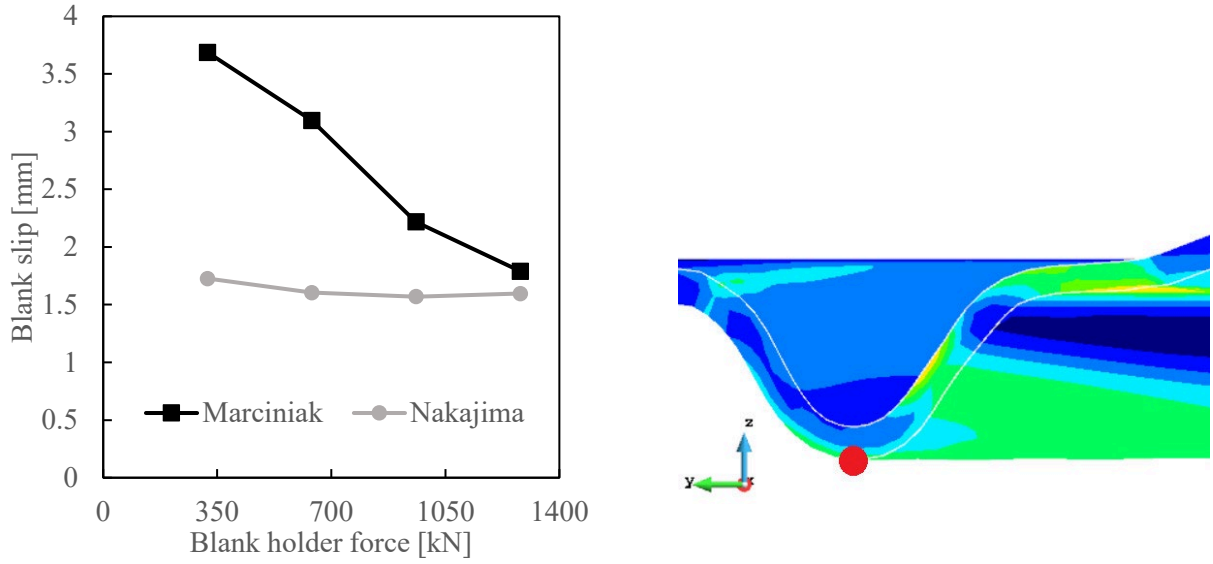

Figure 12. (a) Comparison of blank slip of Marciniak and Nakajima tests with different blank holder forces; (b) Location on the specimen of the point used to evaluate the slip.

The same study was performed for the Nakajima test. However, the effect of the blank holder force was almost negligible in that case, with only a slight deviation in the results for the lower values of blank holder force. The reason for this difference is related with the punch geometry, which induces higher forces in the Marciniak than in the Nakajima (see Fig. 4 (a) and Fig. 7 (a)). Fig. 12 (a) presents the sliding of the blank during the punch movement, evaluated in the radius of the draw bead along the rolling direction (see Fig. 12 (b)), for different values of blank holder force. The Marciniak test presents a significant reduction of the sliding of the blank as the blank holder force increases, while that effect is almost negligible in the Nakajima test.

Influence of the friction coefficient. As in the previous section, the material 0.6_1.8_3 was selected to analyze the influence of the friction coefficient on both tests.

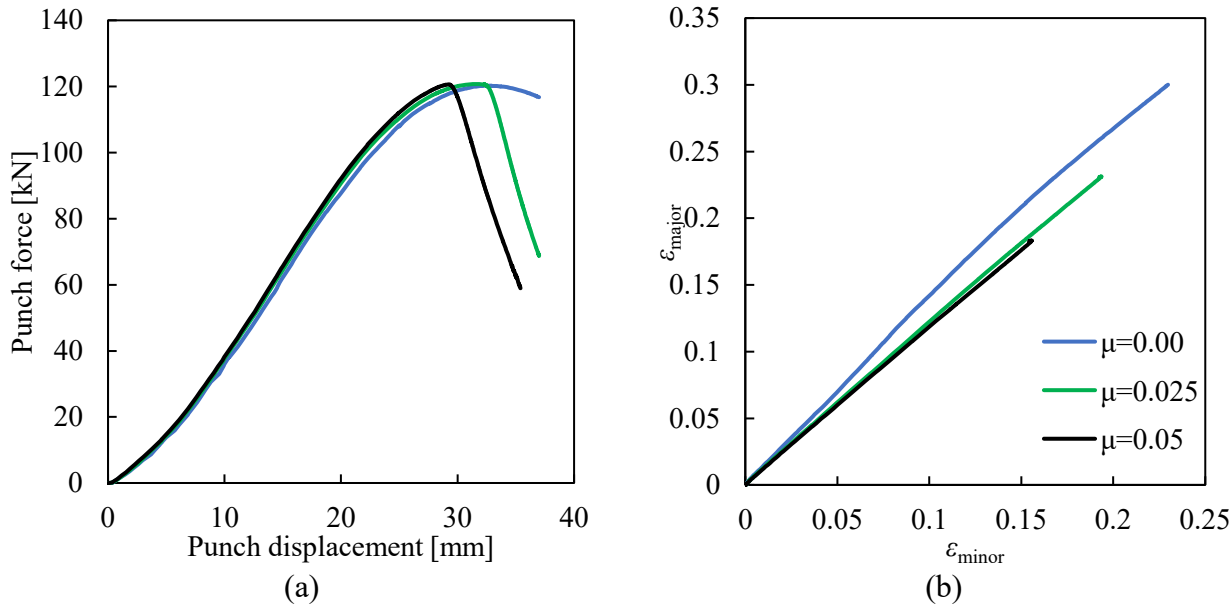

Figure 13. Effect of the friction coefficient on the predictions of the Marciniak test simulations: (a) punch force evolution; (b) major-minor strain.

Regarding the Marciniak test, the increase of the friction coefficient leads to a slight increase of the punch force and to a decrease of the punch displacement for which the maximum force is attained, as shown in Fig. 13 (a). On the other hand, Fig. 13 (b) shows that the strain paths in the center of the blank become more linear.

Fig. 14 (a) and (b) show the effect of the friction coefficient in the stress and strain ratio, respectively. The increase of the friction coefficient caused an increase of both the stress and the strain ratio. Nevertheless, the application of a friction coefficient different from null had a bigger effect than the increase of the coefficient. This effect is related with the change of the contact conditions, which affect the strain distribution. Fig. 15 present the distribution of the equivalent plastic strain for different friction coefficients in the Marciniak specimen, for a punch displacement of 30 mm. The increase of the friction coefficient leads to higher equivalent plastic strain values in the punch shoulder region. Note that for a punch displacement of 30 mm and the higher friction, there is localization in this region (see also Fig. 13 (a)). When the localization starts to occur, the center of the specimen stops to deform. Nevertheless, it should be mentioned that the main purpose of the intermediate blank used in the Marciniak tests, is to minimize friction effects, including the strain localization in the punch shoulder. The fact that the numerical model is neglecting the presence of the intermediate blank means that the influence of the contact with friction conditions are being overestimated.

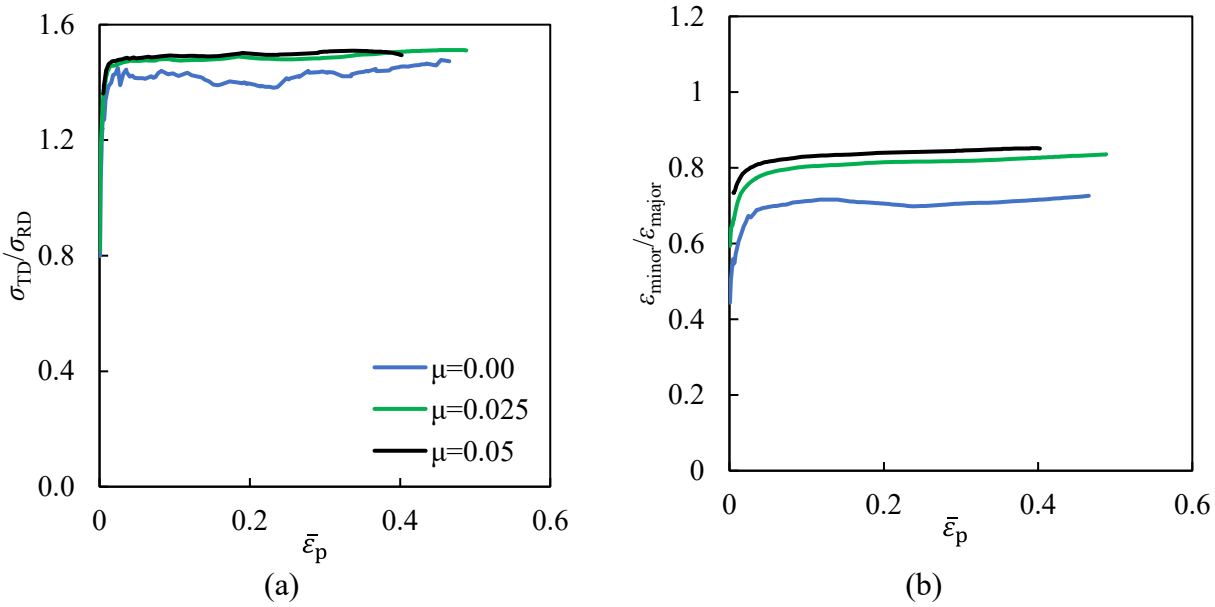

Figure 14. Effect of the friction coefficient on the predictions of the Marciniak test simulations: (a) Stress path ratio- equivalent plastic strain; (b) Strain path ratio- equivalent plastic strain.

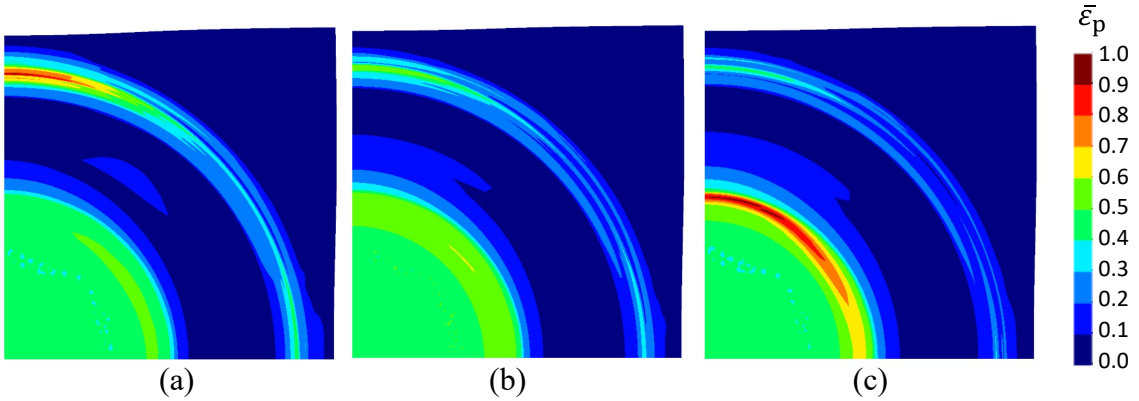

Figure 15. Equivalent plastic strain distribution in the specimen of the Marciniak test, for a punch displacement of 30 mm, with friction coefficient: (a) null; (b) 0.025; (c) 0.05.

Fig. 16 (a) and (b) presents the Nakajima punch force evolution and the strain paths, respectively. As for the Marciniak test, the influence of the friction coefficient in the punch force is negligible but, the strain path presents a strong change from frictionless conditions to the other results. Also, the strain path becomes more linear for higher friction coefficient values.

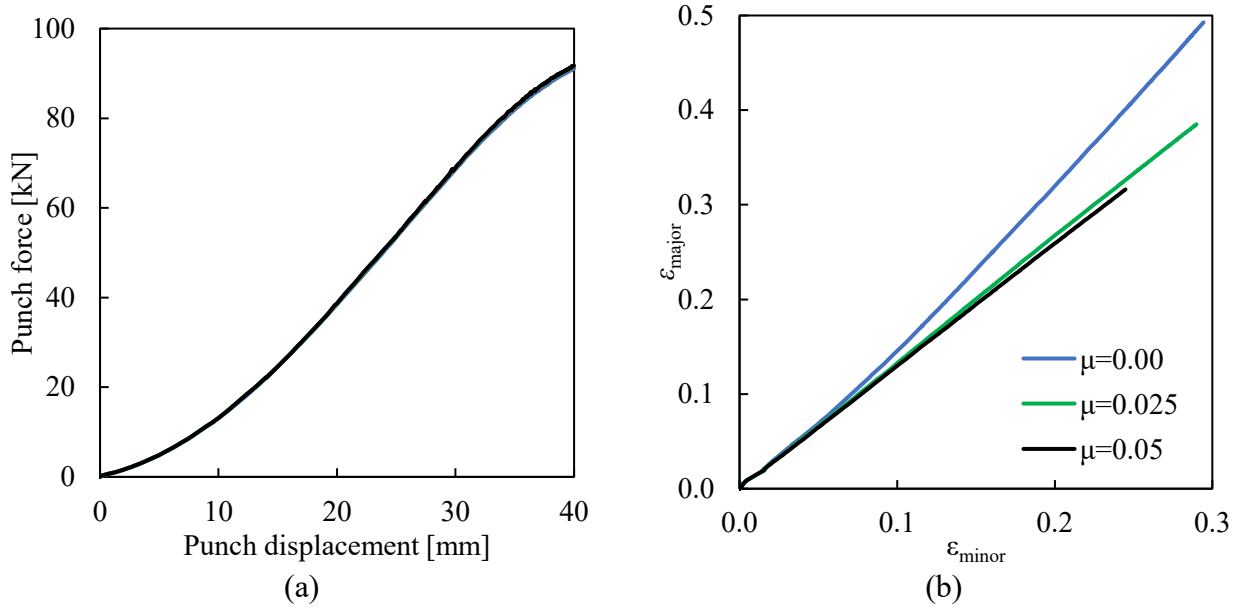

Figure 16. Effect of the friction coefficient on the predictions of the Nakajima test simulations: (a) punch force evolution; (b) major-minor strain.

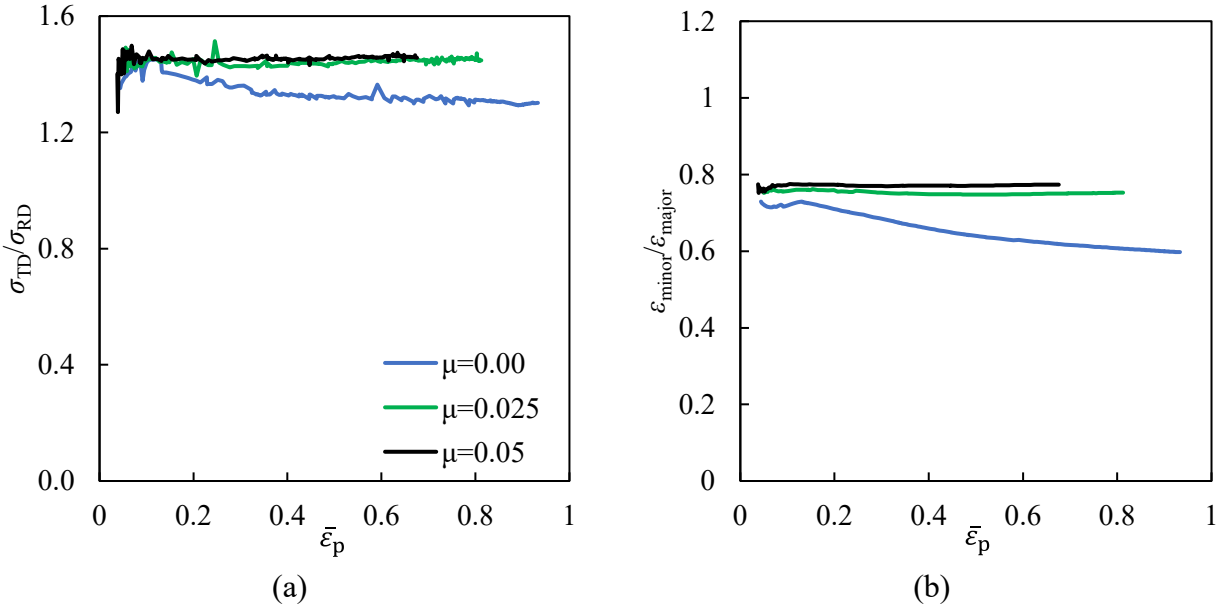

Figure 17. Effect of the friction coefficient on the predictions of the Nakajima test simulations: (a) Stress path ratio- equivalent plastic strain; (b) Strain path ratio- equivalent plastic strain.

Fig. 17 shows the stress and strain ratios evolution for three different values of friction coefficient. Increasing the friction coefficient leads to more linear evolutions, converging to 1.4 and 0.8 for the stress and strain ratio, respectively. As in the Marciniak test, the fact of being frictionless or not presents a greater effect than the increase of the friction coefficient value. This is related with the change of the contact conditions in the punch. Under frictionless conditions, the strain localization occurs in the specimen center, while necking moves from the center with the increase of the friction coefficient, as shown in Fig. 18. When this occurs, the center of the specimen stops to deform, which justifies the decrease of the equivalent plastic strain and the more constant values for the stress and the strain ratios. This is in agreement with the results reported in [12]. Globally, the Nakajima test is more sensitive to changes in the friction coefficient than the Marciniak test.

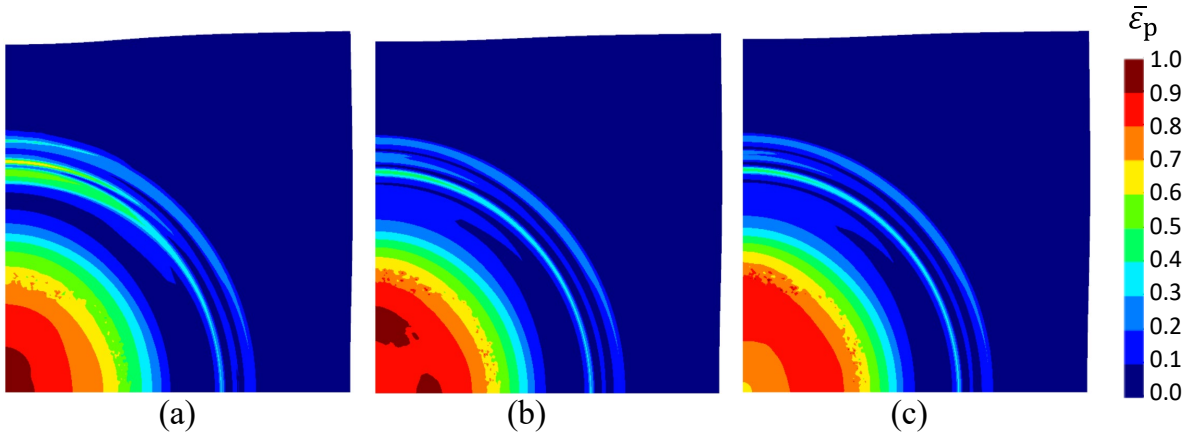

Figure 18. Equivalent plastic strain distribution in the specimen of the Nakajima test, for a punch displacement of 40 mm, with friction coefficient: (a) null; (b) 0.025; (c) 0.05.

Conclusions

The numerical analysis of both Marciniak and Nakajima tests was performed to assess the impact of the material orthotropic behavior on the stress and strain paths, when using a square specimen. Anisotropic materials with $r_0 = r_{90}$ showed a behavior similar to that of the isotropic material, with the specimen center in equibiaxial stress and strain. Materials with a high degree of anisotropy present stress and strain paths which are not equibiaxial, because these occur for different positions in the yield surface. Therefore, in these cases, the stress state achieved is a balance between equibiaxial stress and equibiaxial strain. It is known that the Hill'48 yield criterion adopted in this work does not allow to correctly describe some anisotropic behaviors, including those designated by Banabic as 'first and second order anomalous' behaviors [11]. Those can be described by more flexible yield criteria, leading to similar conclusions, as shown in [9] for the hydraulic expansion test.

The blank holder force had a negligible effect on the Nakajima test but it caused significant changes in the strain paths of the Marciniak test. This effect was caused by blank slippage, highlighting the importance of assuring the proper control of the blank displacement, particularly in the Marciniak test. On the other hand, the Nakajima test is more sensitive to small changes in the friction coefficient value, because it affects the location of the necking (it occurs in the center of the blank only for frictionless conditions). The Lode parameter is more sensitive to small changes in the stress ratio than the stress triaxiality. The differences observed from their reference values for equibiaxial stress state should be taken into account when analyzing forming limit results.

Acknowledgements

The authors gratefully acknowledge the financial support of the projects POCI-01-0145-FEDER-030592 (PTDC/EME-EME/30592/2017) and UIDB/00285/2020 financed by the Operational Program for Competitiveness and Internationalization, in its FEDER/FNR component, and the Portuguese Foundation of Science and Technology (FCT), in its State Budget component (OE).

References

[1] A.S. Wifi, Finite element correction matrices in metal forming analysis (with application to hydrostatic bulging of a circular sheet), Int. J. Mech. Sci. 24 (1982) 393–406. https://doi.org/10.1016/0020-7403(82)90050-9.

[2] A. Khalfallah, J.L. Alves, M.C. Oliveira, L.F. Menezes, Simulation Modelling Practice and Theory Influence of the characteristics of the experimental data set used to identify anisotropy parameters, Stimul. Model. Pract. THEORY. 53 (2015) 15–44. https://doi.org/10.1016/j.simpat.2015.02.007.

[3] D. Ledentsov, A. Düster, W. Volk, M. Wagner, I. Heinle, E. Rank, Model adaptivity for industrial application of sheet metal forming simulation, Finite Elem. Anal. Des. 46 (2010) 585–600. https://doi.org/10.1016/j.finel.2010.02.006.

[4] S.D. Antolovich, R.W. Armstrong, Plastic strain localization in metals: Origins and consequences, Prog. Mater. Sci. 59 (2014) 1–160. https://doi.org/10.1016/j.pmatsci. 2013.06.001.

[5] S.P. Keeler, Circular grid system - A valuable aid for evaluating sheet metal formability, in: SAE Tech. Pap., 1968. https://doi.org/10.4271/680092.

[6] G.M. Goodwin, Application of strain analysis to sheet metal forming problems in the press shop, in: SAE Tech. Pap., 1968: pp. 380–387. https://doi.org/10.4271/680093.

[7] ISO - ISO 12004-2:2021 - Metallic materials — Determination of forming-limit curves for sheet and strip — Part 2: Determination of forming-limit curves in the laboratory, (2021). https://www.iso.org/standard/78138.html.

[8] J. Mulder, H. Vegter, H. Aretz, S. Keller, A.H. Van Den Boogaard, Accurate determination of flow curves using the bulge test with optical measuring systems, J. Mater. Process. Technol. 226 (2015) 169–187. https://doi.org/10.1016/j.jmatprotec.2015.06.034.

[9] L.C. Reis, P.A. Prates, M.C. Oliveira, A.D. Santos, J. V. Fernandes, Anisotropy and plastic flow in the circular bulge test, Int. J. Mech. Sci. (2017). https://doi.org/10.1016/J.IJMECSCI.2017.04.007.

[10] Z. Marciniak, K. Kuczyński, Limit strains in the processes of stretch-forming sheet metal, Int. J. Mech. Sci. 9 (1967) 609–620. https://doi.org/10.1016/0020-7403(67)90066-5.

[11] D. Banabic, Sheet metal forming processes: Constitutive modelling and numerical simulation, Germany: Springer Berlin Heidelberg, 2010. https://doi.org/10.1007/978-3-540-88113-1.

[12] Kasaei, M. M., M.C. Oliveira, Influence of the contact with friction on the deformation behavior of advanced high strength steels in the Nakajima test, J. Strain Anal. Eng. Des. (2021). https://doi.org/10.1177/03093247211021257.

[13] R. Zhang, Z. Shao, J. Lin, A review on modelling techniques for formability prediction of sheet metal forming, Int. J. Light. Mater. Manuf. 1 (2018) 115–125. https://doi.org/10.1016/J.IJLMM.2018.06.003.

[14] H.W. Swift, Plastic instability under plane stress, J. Mech. Phys. Solids. 1 (1952) 1–18. https://doi.org/10.1016/0022-5096(52)90002-1.

[15] K.-H. Chang, e-Design: Computer-Aided Engineering Design, Elsevier Inc., 2015. https://doi.org/https://doi.org/10.1016/B978-0-12-382038-9.12001-0.

[16] R. Hill, A theory of the yielding and plastic flow of anisotropic metals, Proc. R. Soc. London. Ser. A, Math. Phys. Sci. (1948) 281–297. https://doi.org/10.1098/RSPA.1948.0045.

[17] L.F. Menezes, C. Teodosiu, Three-dimensional numerical simulation of the deep-drawing process using solid finite elements, J. Mater. Process. Technol. 97 (2000) 100–106. https://doi.org/10.1016/S0924-0136(99)00345-3.

[18] M.C. Oliveira, J.L. Alves, L.F. Menezes, Algorithms and strategies for treatment of large deformation frictional contact in the numerical simulation of deep drawing process, Arch. Comput. Methods Eng. (2008). https://doi.org/10.1007/S11831-008-9018-X.

[19] T.J.R. Hughes, J. Winget, Finite rotation effects in numerical integration of rate constitutive equations arising in large-deformation analysis, Int. J. Numer. Methods Eng. 15 (1980) 1862–1867. https://doi.org/10.1002/NME.1620151210.

[20] D.M. Neto, M.C. Oliveira, J.L. Alves, L.F. Menezes, Comparing faceted and smoothed tool surface descriptions in sheet metal forming simulation, Int. J. Mater. Form. 8 (2015) 549–565. https://doi.org/10.1007/S12289-014-1177-8/FIGURES/21.

[21] D.M. Neto, Numerical simulation of frictional contact problems using Nagata patches in surface smoothing, Coimbra University, 2014.

[22] M.C. Oliveira, D.M. Neto, J.L. Alves, L.F. Menezes, Study on the influence of the yield surface shape in the hole expansion test, IOP Conf. Ser. Mater. Sci. Eng. (2020). https://doi.org/10.1088/1757-899X/967/1/012085.